IEEE Robotics and Automation Letters (RA-L) paper, presented at ICRA 2023, London, UK. Cite as RA-L paper.

S^{2}worm: A Fast-moving Untethered Insect-scale Robot with 2-DoF Transmission Mechanism

Yide Liu, Yanhong Chen, Bo Feng, Dongqi Wang, Taishan Liu, Haofei Zhou, Hua Li, Shaoxing Qu and Wei Yang

***Abstract*— Designing terrestrial insect-scale robot with high maneuverability and autonomy is becoming an essential challenge in the field of robotics research. Previous work has indicated that compact transmission and integrated control devices can improve the application potential. In this work, an untethered insect-scale inchworm robot is designed and fabricated by using screw theory and smart composite microstructure method, and is named S^{2}worm. The robot weighs 4.34 g and spans 4.1 cm in length. The robot is equipped with custom designed onboard control system and high voltage boost converter to provide the driving signal for the piezoelectric bending actuator. Attributing to the novel transmission mechanism with two degrees of freedom designed based on screw theory, the S^{2}worm can be fabricated through the smart composite microstructure method easily and shows high mobility such as high crawling speed (27.4 cm/s, 6.7 body length/s) and small turning radius (1.7 cm, 0.4 body length/s). The S^{2}worm holds the following advantages: small size, untethered, high mobility and low energy consumption. The robot is promising for application in planetary exploration, earthquake search and constructing insect-scale multi-robot system.**

***Index Terms*—Micro/nano robots, biologically-inspired robots, parallel robots, screw theory**

I. INTRODUCTION

Tiny robots generally take inspiration from natural insects such as inchworm [1], bee [2] and cockroach [3]–[5]. These researches promote the theories and methods of design and manufacture. Among all these robots, the terrestrial insect-scale robot is one of the major directions which holds the advantages such as high maneuverability, fast locomotion and terrain adaptability [6].

Most of the terrestrial insect-scale robots can be simplified into an artificial mechanical system that is composed of a driving mechanism working as bones and muscles and autonomous devices working as the brain. In contrast to a large-scale robot, the design and fabrication process of the insect-scale robot seldom adopts traditional methodologies and off-the-shelf components. For instance, instead of actuators such as motors, pneumatic and hydraulic actuators widely used in large-scale robots, the most popular actuation components in insect-scale robots are electromechanical motors [7]–[9] and smart materials such as piezoelectric ceramic [2], [10], dielectric elastomer [11], [12], and shape memory alloy [3], [13].

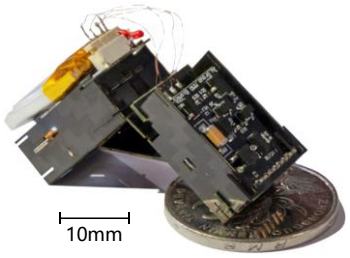

Fig. 1. Photograph of S^{2}worm. A 2-DoF insect-scale inchworm like robot fabricated through SCM method. The robot is equipped with a double deck PZT actuator to drive the 2-DoF transmission designed by screw theory. The S^{2}worm is equipped with onboard power and control electronics to achieve untethered locomotion. A coin is included for scale.

The transmission mechanism is another challenge. The response of smart material actuators generally takes the form of deformation rather than rotatory motion, and linkage mechanisms are employed to transfer the deformation into the motion of robots. [3], [10], [14]. Moreover, to mimic the real joint motion of the insect, more than one Degree of Freedom (DoF) of the transmission mechanism is required. A successful example is the Spherical Five Bar (SFB) mechanism, a well-known 2-DoF transmission mechanism, which has been applied on HAMR series robots as hip joints [15]. Ascribed to the outstanding performance of the SFB, HAMR can run and make turns quickly. For inchworm like robots, soft robots at insect-scale can make turns by activating their muscles asymmetrically [11], [12], while the robots with hard structures can seldom make turns. Accordingly, to achieve the high mobility of an inchworm like robot, a 2-DoF transmission mechanism for inchworm robot is needed. To achieve such a compact mechanism at small scale, parallel mechanism is preferred rather than the series mechanism due to its compact structure, high rigidity and fast speed. A parallel mechanism is one in which two or more serial kinematic chains connect the moving platform to the base. Its high rigidity is attributed to the multiple supports of the limbs when the moving platform is loaded. However, this requirement leads to difficulty in the design since there is no appropriate reference of the 2-DoF parallel mechanism besides the SFB.

Manuscript received: December 28, 2021; Revised: March 13, 2022; Accepted: May 5, 2022.

This paper was recommended for publication by Editor Xinyu Liu upon evaluation of the Associate Editor and Reviewers' comments. This work is supported by the National Natural Science Foundation of China (No. 91748209).

All the authors are with the Department of Engineering Mechanics, Zhejiang University, 310027 China. (corresponding author to provide e-mail: squ@zju.edu.cn (Shaoxing Qu)).

Digital Object Identifier (DOI): see top of this page.

Several methods were proposed to fabricate the tiny mechanism, such as smart composite microstructure (SCM) method [4], [16], [10], [17], silicon on insulator (SOI) process [14], [18]–[21], 3D printing [22] and so on. The control system of the insect-scale robot must base on its hardware design. The autonomy of the insect-scale robot plays an important role in real applications. While equipping onboard electronics brings difficulties since the electronics for driving the robot are heavier than the insect-scale robot istself [6].

To achieve the high maneuverability and autonomy of the insect-scale robot, we aim to build an untethered terrestrial inchworm robot with a 2-DoF mechanism and onboard electronics to achieve universal locomotion (move forward and make turns). Crawling approach is chosen for the motivations as:

(1). Crawling approach only need two DoFs to achieve universal locomotion. Less DoFs will be convenience for fabrication and control process. This will also compress the robot size and simplify the control scheme.

(2) Our future target is constructing a quadruped robot system assembled from eight inchworm-like robots, the BioARS system [23]. Considering from this aspect, we prefer to design a small robot with universal locomotion ability while acts like a joint of an animal's limb.

We develop a novel 2-DoF transmission mechanism based on the *screw theory* and build an inchworm robot driven by this mechanism following the SCM method. The robot is named S^{2}worm (Fig. 1). We demonstrate the type synthesis and mobility analysis through screw theory and we discuss the importance of applying screw theory in limbs design of the mechanism for the following SCM fabrication process. Actuation is provided by a double deck PZT actuator. The integrated electronics provide onboard power and onboard motion control. The robot can be controlled by the host computer remotely through the integrated WiFi module. Attributing to the 2-DoF mechanism and onboard electronics, the untethered robot can achieve universal locomotion. The S^{2}worm shows high mobility such as high crawling speed (27.4 cm/s, 6.7 body length/s) and small turning radius (1.7 cm, 0.4 body length).

II. Design and Fabrication

A. Type Synthesis and mobility analysis

To achieve the universal locomotion of an insect-scale crwaling robot, we intend to design the transmission mechanism of the robot with 2-DoF. For an insect-scale robot, the transmission mechanism is preferred to be a parallel mechanism since they have higher rigidity. According to the survey, 2-DoF parallel mechanism design is relatively rare [24]. The reasons that the SFB is not applied in this work and we design a novel 2-DoF transmission mechanism are:

(1) Coupling feature: the SFB is a better fit for legged micro robot since its 2 DoFs are decoupled and the foot trajectory can be designed conveniently in this mechanism. As for a crawling robot, we prefer a coupling feature when the robot is moving forward for higher efficacy, and the

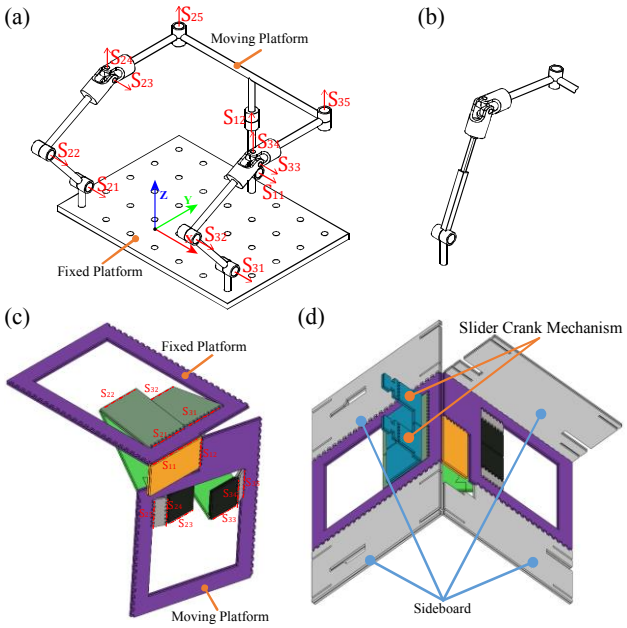

Fig. 2. Structure and transmission of the S^{2}worm. A 2-DoF parallel mechanism constructed with an exoskeleton limb and two muscle limbs. (a). The schematic of the 2-DoF transmission mechanism. (b). The schematic of another possible limb structure based on the twist system of equation (4) which contains a prismatic joint. (c). The CAD model of the transmission of the S^{2}worm. (d). The whole mechanical structure of the S^{2}worm including the 2-DoF parallel mechanism, two slider crank mechanisms and four sideboards.

mechanism we designed has two identical limbs for providing driving force.

(2) Rigidity: we want one more passive limb for proving constraint force to promote the rigidity of the mechanism. Many insects evolved exoskeletons to offer body support and motion constraint. To mimic this nature design, the passive limbs possesses similar function as the exoskeleton.

Thus, the target is to design a 2-DoF transmission mechanism with three limbs. One for the exoskeleton and the other two for actuation as muscles identically. A common idea to create a n-DoF mechanism with n+1 limbs is to combine n 6-DoF limbs for actuation and a n-DoF limb for constraint together [25]. This design is similar to our target, but there exists a serious issue in the 6-DoF limb. Because the 6-DoF limb cannot offer constraint force, this type of design is lacking in rigidity. Therefore, to achieve the high mobility transmission mechanism of the insect-scale robot, an original 2-DoF mechanism with exoskeleton-like limb for structure support need to be designed. The powerful tool for the designing process we introduced is screw theory, which is applied herein to demonstrate the type synthesis and mobility analysis of the mechanism [26]–[28].

The 2-DoF parallel mechanism we performed in this work has two rotational DoFs and three limbs (Fig. 2(a)). The limbs of the mechanism can be named exoskeleton limb and muscle limbs. The exoskeleton limb offers the motion constraint and the two muscle limbs offer the actuation.

The standard base of the twist system [28] of the 2-DoF mechanism is chosen as：

$$\begin{aligned} S_1 &= (1,0,0;0,0,0) \\ S_2 &= (0,c\theta,s\theta;0,0,0) \end{aligned} \tag{1}$$

where $s\theta$ and $c\theta$ represent $\sin\theta$ and $\cos\theta$ for brevity, θ is the angle of the rotational motion along S_1

In the mechanism twist system, S_1 and S_2 can construct a universal joint. The twist system of the exoskeleton limb is formed because it is equal to the mechanism twist system. The three extra twists we add to the muscle limb twist systems are:

$$\begin{aligned} S_3 &= (0,0,0;1,0,0) \\ S_4 &= (0,0,0;0,1,0) \\ S_5 &= (0,0,0;0,0,1) \end{aligned} \tag{2}$$

These three twists are three translation motions, while we prefer to construct a revolute joint in the SCM fabrication process, thus we choose the linear combination of the above five twists as:

$$\begin{aligned} S_1 &= (1,0,0;0,0,0) \\ S_2 &= (1,0,0;0,b_2,c_2) \\ S_3 &= (1,0,0;0,b_3,c_3) \\ S_4 &= (0,c\theta,s\theta;a_4,b_4,c_4) \\ S_5 &= (0,c\theta,s\theta;a_5,b_5,c_5) \end{aligned} \tag{3}$$

According to the twist system in eq. (3), we can construct the muscle limb kinematic chain. The first three revolute joints are parallel to each other, and the last two revolute joints are parallel to each other. The third revolute axis and the fourth revolute axis are designed to intersect together, which assimilated to a universal joint, thus can simplify the manufacturing process. The 2-DoF 3 limbs mechanism of this design is shown in Fig. 2(a).

The main thing to be emphasized here is that the choice of the linear combination of the limbs in equation (3) is not random but after a careful consideration. To simplify the SCM fabrication process, the structure of the mechanism should be easy to planarization. A counter example is that the linear combination of the twist system of the muscle limb can also be chosen as:

$$\begin{aligned} S_1 &= (1,0,0;0,0,0) \\ S_2 &= (0,0,0;0,c\alpha,s\alpha) \\ S_3 &= (1,0,0;0,b_3,c_3) \\ S_4 &= (0,c\theta,s\theta;a_4,b_4,c_4) \\ S_5 &= (0,c\theta,s\theta;a_5,b_5,c_5) \end{aligned} \tag{4}$$

The above twist system refers to a limb including a prismatic joint which is shown in Fig. 2 (b). Compared with the muscle limb in Fig.2 (a) , both of them can achieve the 2-DoF parallel mechanism, while the limb from equation (4) is inconvenient to fabricate since the prismatic joint need to be replaced by a Sarrus linkage in the SCM process [16]. It verifies that the application of the screw theory can solve the design and fabrication problem of SCM method by choosing the combination of the limb twist system. An appropriate combination can eliminate the prismatic joints or replace the prismatic joints with revolute joints, which is a vast simplification to the following fabrication.

Based on the above design, the twist system of the exoskeleton limb l_1 can be written as:

$$\mathrm{S}_{l1} = \begin{Bmatrix} S_{11} = (1,0,0;0,0,-L_{11}) \\ S_{12} = (0,c\theta,s\theta;L_{11}s\theta,0,0) \end{Bmatrix} \tag{5}$$

where L_{11} is the distance from the origin to the intersection of S_{11} and S_{12}. The origin passes the line of S_{21} and S_{31}.

According to screw theory of the parallel mechanism, all wrenches of the constraint system should be reciprocal to the twist of the twist system [28], [29]. The constraint system S^r_{l1} of the exoskeleton limb l_1 is calculated as:

$$\mathrm{S}^r_{l1} = \begin{Bmatrix} S^r_{11} = (0,0,1;L_{11},0,0) \\ S^r_{12} = (1,0,0;0,0,-L_{11}) \\ S^r_{13} = (0,1,0;0,0,0) \\ S^r_{14} = (0,0,0;0,-s\theta,c\theta) \end{Bmatrix} \tag{6}$$

The twist systems of the muscle limbs $\mathrm{S}_{\overline{l2}}$ and $\mathrm{S}_{\overline{l3}}$ are written as:

$$\mathrm{S}_{li} = \begin{Bmatrix} S_{i1} = (1,0,0;0,0,0) \\ S_{i2} = (1,0,0;0,q_2,r_2) \\ S_{i3} = (1,0,0;0,q_3,r_3) \\ S_{i4} = (0,c\theta,s\theta;p_5,q_5,r_5) \\ S_{i5} = (0,c\theta,s\theta;p_6,q_6,r_6) \end{Bmatrix} (i=2,3) \tag{7}$$

And the constraint system for limbs l_2 and l_3 are:

$$\mathrm{S}^r_{li} = S^r_{i1} = (0,0,0;0,-s\theta,c\theta)(i=2,3) \tag{8}$$

It is apparently that $\mathrm{S}^r_{\overline{l2}}$ and $\mathrm{S}^r_{\overline{l3}}$ are subsets of $\mathrm{S}^r_{\overline{l1}}$. Since the constraint system $\mathrm{S}^r_{\underline{\ }}$ of the moving platform is the union of all limbs constraint system, $\mathrm{S}^r_{\underline{\ }}$ is calculated as:

$$\mathrm{S}^r = \mathrm{S}^r_{l1} \cup \mathrm{S}^r_{l2} \cup \mathrm{S}^r_{l3} = \mathrm{S}^r_{l1} \tag{9}$$

Thus, the twist system of the moving platform $\mathrm{S}_{\overline{f}}$ which contains a combination of the twists reciprocal to the wrenches in the constraint system and is also the intersection of the limbs twist system is calculated as:

$$\mathrm{S}_f = S_{l1} \cap S_{l2} \cap S_{l3} = S_{l1} \tag{10}$$

Equation (10) confirms that the moving platform has two DoFs. The mobility of the moving platform is equal to the mobility of the exoskeleton limb l_1.

We applied the general Grübler-Kutzbach criterion to check the mobility [29]. By considering the over-constrained effects, including common constraint and passive constraint, the criterion is stated as follows:

$$M = d(n-g-1) + \sum_{i=1}^{g} f_i + v \tag{11}$$

where M is the mobility of the mechanism, d represents the order of the mechanism, $d = 6-\lambda$, with λ being the number of common constraints, n is the number of links, g is the number of kinematic pairs, f_i denotes the freedom of the i-th pair, and v is the number of the passive constraints.

Based on equations (6) and (8), the constraint systems of all three limbs have a common constraint wrench,

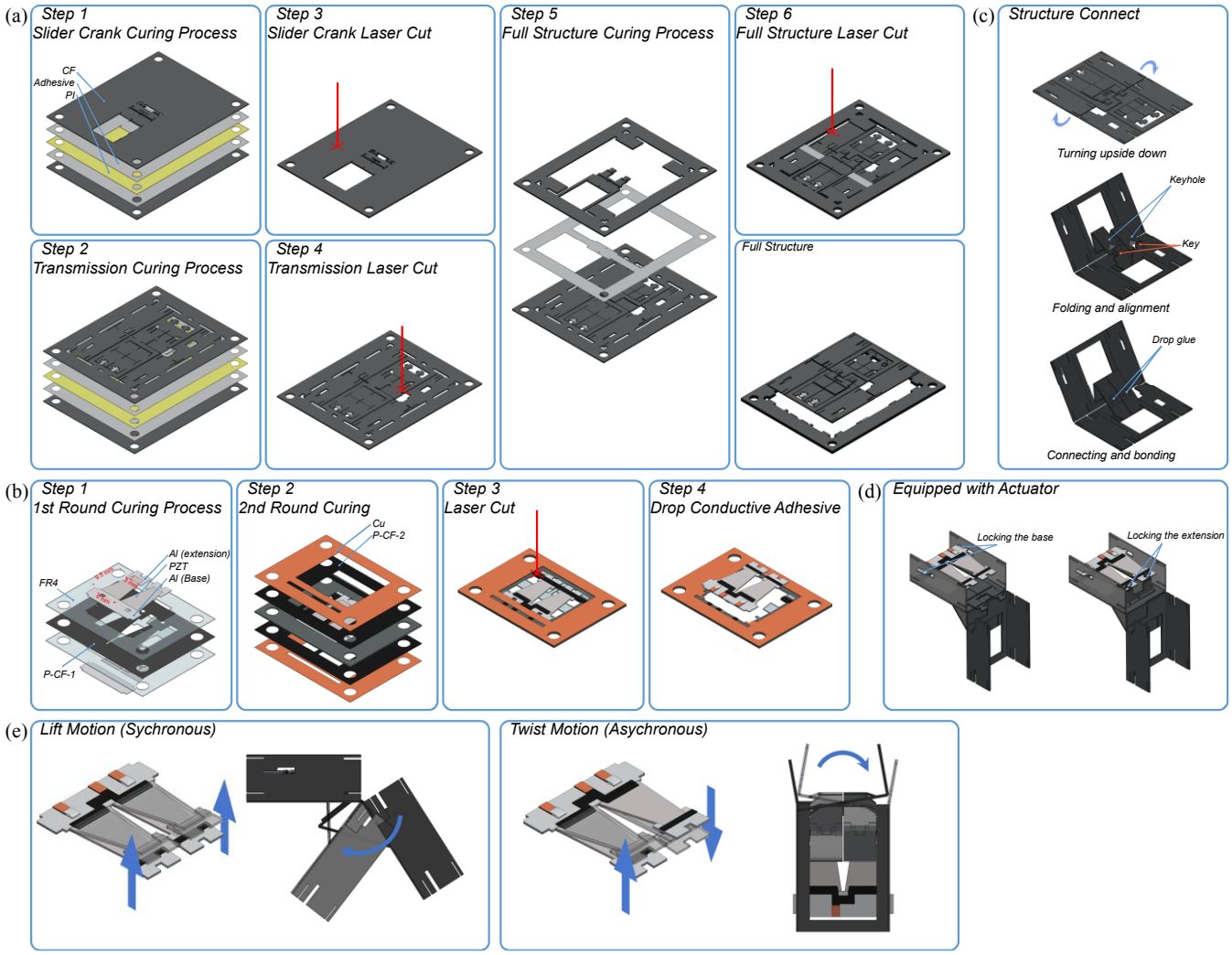

Fig. 3. The fabrication process, assembly process and kinematics of the S^{2}worm. (a) The fabrication process of the structure of the S^{2}worm. (b) The fabrication process of the double deck PZT actuator. (c) The assembly process of the structure. To fabricate a 2-DoF close loop transmission through SCM method, a pair of bars are broken. To repair these bars, we design keys and keyholes to help align and bond them by glue. (d) The assembly process of the actuator. The base of the actuator is locked with the sideboards and the extensions are locked with the slider crank mechanisms. (e) The kinematics of the 2-DoF transmission. When the double decks of the actuator are driven synchronously, the transmission performs lift motion. When the double decks of the actuator are driven asynchronously, the transmission performs twist motion.

$(0,0,0;0,-s\theta,c\theta)$ .This screw is a pure torque reciprocal to all the twists associated with the kinematic pairs in the proposed mechanism. Thus, the number of the common constraint λ equals one and the order of the mechanism is $d=6-1=5$. The mobility of the mechanism is given as:

$$M=5(11-12-1)+12+0=2 \tag{12}$$

Several extra components are added for actuation and assembly (Fig. 2(d)). The actuation forces of the robot are generated from the PZT actuator. Two slider crank mechanisms are added to the muscle limbs on the blackish green bars between S_{i1} and S_{i2} (i =2,3). Four sideboards are added on the fixed platform and moving platform for assembling the actuators and electronics.

B. Structure fabrication and kinematics

The applications of SCM run through micro robot researches in the last decade. In this work, we adopt the SCM methods to fabricate the body and the piezoelectric actuator of the S^{2}worm (Figs. 3(a) and (b)). All components of the SCM b method for constructing the mechanisms and actuators are listed in Table I. Moreover, to achieve the parallel mechanism of the robot structure, as mentioned before, we adopt the method to create male keys and female keyholes on carbon fiber frames to help break and reconnect the bars between S_{i2} and S_{i3} (i=2,3) [30] (Fig. 2(d) and Fig. 3(c)).

For the whole carbon structure of the S^{2}worm, individual layers are patterned by laser and then cured under heat and pressure for bonding. The structure of the S^{2}worm contains a 2-DoF parallel mechanism as main transmission and two slider crank mechanisms. We fabricate these two laminates separately (Fig. 3(a) Step 1-4). After that, an adhesive sheet is introduced between these two laminates to bond. The deck above is then cured and cut out of the frame to create the whole structure of the S^{2}worm body (Fig. 3(a) Step 5-6).

The double deck PZT actuator contains piezoelectric ceramic (PZT-5H, piezo.com), alumina ceramic, two types of carbon fiber prepregs with different thicknesses and copper foil. The epoxy glass cloth (FR4) is laser machined as the frame to fix the ceramics. The deck is shown in Fig.3(b) Step 1, with the piezoelectric ceramics placed between the alumina ceramics in the same layer. The piezoelectric ceramics are coated with silver on both sides as conductor. The alumina ceramics are cut as the bases and the extensions. A 50 μm carbon fiber prepreg sheet is patterned and sandwiched by two FR4 sheets. After curing, the whole deck is sandwiched by two 200 μm carbon fiber prepreg sheets and copper foils. We cure the new deck and cut it out of the frame to get the piezoelectric actuator (Fig. 3 (b) Step 2-3). A small amount of conductive adhesive is dropped to fill the hole on the alumina ceramic base to connect the middle layer 50 μm carbon fiber prepreg and the top layer copper electrode (Fig. 3(b) Step 4).

We equipped the structure of the robot with the actuator by fixing the base of the actuator on the sideboards and connecting the extensions to the slider crank mechanisms (Fig. 3(c) and (d)). All the connections are locked by glue. The piezoelectric actuator has two decks to drive the slider crank mechanisms and the respective muscle limbs of the 2-DoF transmission individually. The lift motion of the S²worm is driven by the decks synchronously, and the twist motion is driven by the decks asynchronously (Fig. 3(e)).

C. *Power, Control and actuation*

The power and control system need to be designed to meet the high driven voltage and the centimeter scaled body of the S²worm. A 3.7 V 35 mAh rechargeable lithium battery is chosen as the power source. The onboard electronics contain the onboard controller and the high voltage boost converter (Fig. 4(a)). The onboard controller can receive the commands from the host computer and adjust the output of the boost converter through three PWM signals. The boost converter mainly consists of a Flyback converter for providing high voltage and two complementary push-pull circuits for producing two channel control signals for the two decks of the PZT actuator. Components of the electronic circuit in Fig. 4(a) are list in Table II.

The simultaneous configuration is applied here to achieve the electrical contacting of the double deck PZT actuator [31]. The passive flexible carbon fiber is embraced symmetrically by two active piezoelectric ceramics. The high voltage amplifier offers four wires: a common 300V bias wire, a common ground wire and two 0-300V driving signal wires for driving the left and the right decks of the actuator independently (Fig. 4(b) and (c)).

We used two idealized 20 Hz sinusoidal signals with T/2 phase difference as driving signals to explain the driving principle of the actuator. A deck contains two pieces of PZT ceramics, the driving voltage of the top PZT could be calculated as the difference between the bias voltage and the driving signal. The driving voltage of the bottom PZT could be calculated as the difference between the driving signal and the ground voltage. Thus, the driving voltage of the left top, left bottom, right top and right bottom PZTs could be written as:

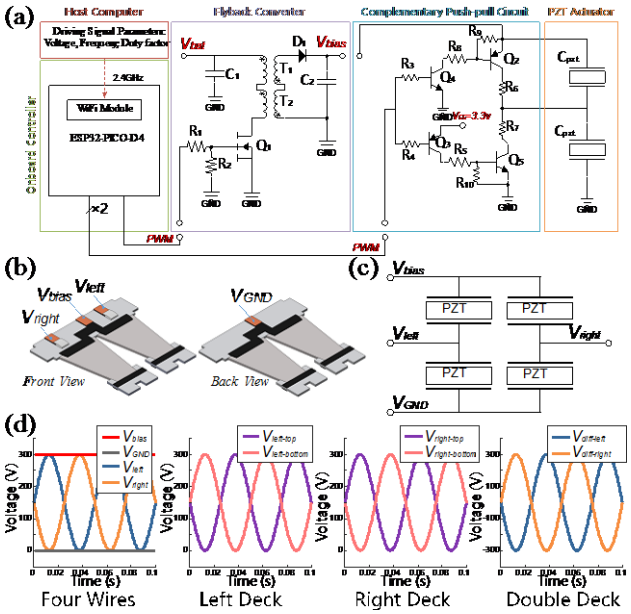

Fig. 4. (a) Circuit schematic of the onboard electronics. The onboard controlled communicate with the host computer through the integrated WiFi module. (b) Electrical contacts of the double deck PZT actuator. (c) Driving diagram of the double deck PZT actuator. (d) Driving signals of the four wires. Two idealized 20 Hz 300V sinusoidal signals are set as drive signals for the double decks to generate asynchronous motion of the actuator.

TABLE I
THICKNESS OF THE COMPONENTS OF THE S²WORM

Component	Abbreviation	Thickness(μm)
Carbon Fiber	CF	200
DuPont FR1500 Sheet Adhesive	Adhesive	12.5
Polyimide Film	PI	7.5
Epoxy Glass Cloth	FR4	127
Piezoelectric Ceramic	PZT	127
Alumina Ceramic	Al	200
Carbon Fiber Prepreg 1	P-CF-1	50
Carbon Fiber Prepreg 2	P-CF-2	200
Copper Foil	Cu	13

TABLE II
COMPONENTS OF THE ELECTRONIC CIRCUIT

Component	Notation	Parameters and model
Capacitor	C_1, C_2	1uF (0402), 1uF (2220)
Resistor	R_1, R_2, R_3 - R_7, R_8, R_9, R_{10}	200Ω, 20kΩ, 10kΩ, 15MΩ, 499kΩ, 100kΩ (All 0402)
Diode	D_1	US1NWF-7
Transformer	T_1, T_2	ATB322515-0110-T000
MOSFET	Q_1	SI2324DS-T1-GE3
PNP	Q_2, Q_3	STR2550
NPN	Q_4, Q_5	STR1550

TABLE III
MASS DISTRIBUTION OF THE S²WORM

Part	Mass(g)
Structure and transmission	0.80
Piezoelectric Actuator	0.28
Battery	1.48
Onboard electronics	1.51
Wires, Solder and Glue	0.27
Total	4.34

$$\begin{aligned} V_{left-top} &= V_{bias} - V_{left} \\ V_{left-bottom} &= V_{left} - V_{GND} \\ V_{right-top} &= V_{bias} - V_{right} \\ V_{right-bottom} &= V_{right} - V_{GND} \end{aligned} \tag{13}$$

To describe the relationship between the driving signals and the deflection, a variable V_{diff} is defined as the differences between the voltage of the top and bottom PZTs. In our configuration, V_{diff} for the decks could be written as:

$$\begin{aligned} V_{diff-left} &= V_{left-top} - V_{left-bottom} = V_{bias} - 2V_{left} \\ V_{diff-right} &= V_{right-top} - V_{right-bottom} = V_{bias} - 2V_{right} \end{aligned} \tag{14}$$

As shown in Fig. 4 (c), the $V_{diff-left}$ and $V_{diff-right}$ hold the same phase differences as the V_{left} and V_{right}, which implies that the phase of the motion can be controlled by adjusting the driving signal of the decks.

Thus, the inchworm contains four major parts, the robot body, the double deck PZT actuator, the battery, and the onboard electronics. Besides, there are some connecting wires and solder. The total mass of an inchworm robot is 4.34g. The mass contributions of each part are listed in Table III.

III. Experimental Results and Discussion

A. Characterizations of PZT actuator

We measure the maximum free deflection of the PZT actuator. The driving signals are set as square waves and the test voltage ranges from 150 V to 250 V. The test frequency ranges from 10 Hz to 100 Hz. The free deflection of the actuator is captured by a laser sensor (LK-G10, KEYENCE). The results are plotted in Fig. 5.

During the deflection measurement, we observe that the shape of the deflection curve changes as the test frequency increases (Figs. 5(b) and (c)). The free deflection is calculated through the peak to peak displacement. A maximum free deflection of nearly 640 μm occurs at 10 Hz, 250 V. The free deflection drops as the voltage drops as well as the test frequency increases.

B. Mobility test of the S²worm

The mobility test of the S²worm mainly focuses on the crawling speed and turning radius. Crawling speed is one of the most important performances of the terrestrial insect robot. The crawling speed of the S²worm driven by onboard electronics is tested with selected voltages of 200 V, 225 V, and 250 V. The crawling speed is recorded in Figs. 6(a). The test surface is an alumina plate which has a static coefficient of friction of approximately 0.4 between the robot and the surface. Reported speeds are averaged for each 10cm steady forward trial.

The maximum speed at 250 V 60 Hz reaches 27.4 cm/s, which is a significant improvement for untethered insect scale robots. Crawling speeds at 50 Hz and 60 Hz are higher than those with the other frequencies. This may relate to the resonance of the actuation and transmission mechanism.

Making turns is another important metric for the terrestrial robot. Insects can make turns in confined spaces. So, the insect-scale robot should be designed with less turning radius.

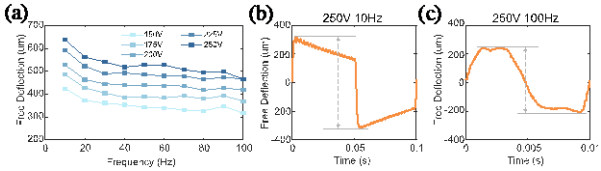

Fig. 5. (a) The free deflection of the double deck PZT actuator under different driving signals. (b) Deflection vs time curve at 250 V 10Hz. The maximum deflection occurs at the beginning of the half cycle and decreases in time. (c) Deflection vs time curve at 250 V 100 Hz. The maximum deflection occurs at the middle of the half cycle.

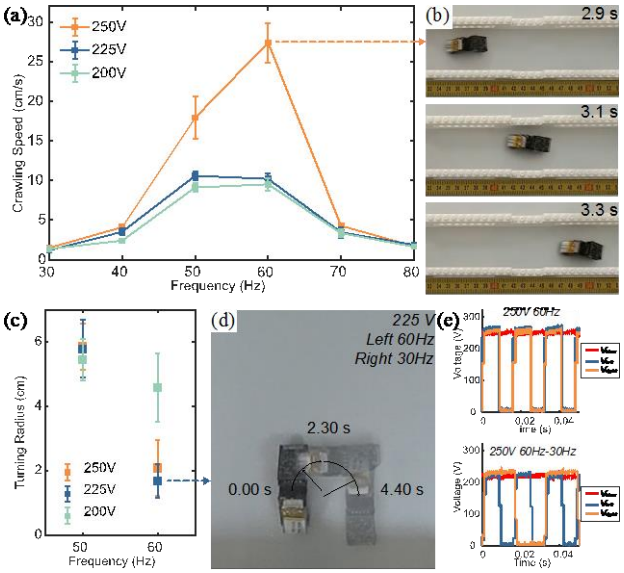

Fig. 6. Mobility test of the S²worm. (a) Crawling speed vs. frequency. Each point is the average speed for a 10 cm steady trial with one standard deviation error bars. (b) Three snapshots of the S²worm to pass 12 cm within 0.4 s. (c) Turning radius vs. frequency. Each point is measured for a 90° turn of the S²worm. (d) Three snapshots of the S²worm to make a 180° U turn within 4.4 s. (e) Onboard drive signals of the S²worm at maximum speed 250 V 60 Hz (upper) and minimum turning radius 225 V 60 Hz-30 Hz (lower) respectively.

In this work, the turning of the S²worm is achieved by adjusting the frequency of the double deck PZT actuator. As demonstrated in section II. C, the double deck PZT actuator is a simultaneous diagram with two driving signals for both sides. To make a right turn, we set the driving signal of the left deck as 200 V 50 Hz while the right deck is 200 V 25Hz. The transmission will produce more propulsion to turn right.

We recorded several groups of turning radius at 50Hz and 60Hz for one side and 25 Hz and 30 Hz for the other side respectively (Fig. 6(c)). All the test parameters produce a steady turning motion. The minimum average turning radius is 1.7 cm at 225V 60 Hz-30 Hz (Figs.6 (d) and (e)).

C. Energy and Cost of Transport

Energy consumption is an important aspect to evaluate the overall performance of a robot. To calculate the energy consumption of the S²worm, we measured two metrics: the energy required to move 1 m and the cost of transport (CoT).

The crawling speeds are selected as 10.6 cm/s, 17.9 cm/s and 27.4 cm/s. We recorded the average current during driving the robot at the above speeds. Test conditions and results are listed in Table IV. The power consumption for S²worm at its

maximum speed is 610.5mW, the equivalent energy to move 1m is 2.23 J and the CoT is 52.4.

We can estimate the endurance of the S²worm through the capacity of the battery. The battery voltage is 3.7 V and the capacity is 35 mAh. The total energy is calculated as $3.7V \times 35mAh = 466.2J$. Based on the energy to move 1m at 27.4 cm/s, the allowable travel distance of the S²worm is ~208 m.

D. Discussion

Surface roughness effects the velocity of our robot. The locomotion principle of the S²worm robot can be explained by the two-anchor crawling model. The propulsive force is generated through the static friction during the lift motion cycle of the robot, thus, the robot moves faster on the relatively rough surface. But too high surface roughness will also block the robot. During the navigation, the robot is driven under a relative high frequency and the two PZT decks cannot perform ideal deflection. This leads to impact force between the robot and the ground, which will induce random undulations.

To compare our results with other robots and insects at a similar scale, five metrics proposed by Ryan St. Pierre and Sarah Bergbreiter in their recent review [6] are followed, which are: the autonomy score, absolute speed, relative speed, energy to move 1m and cost of transport. The S²worm has onboard power and control devices, thus the autonomy score is two. The absolute speed is 27.4 cm/s and the equivalent relative speed is 6.7 body-length per second. Energy to move 1m at 27.4 cm/s is 2.23 J and the CoT is 52.4. We add the above data on the map from the review. Some other robots [32]–[35] and insects [36]–[41] mentioned in the review are added for comparison. It could be found that the S²worm is one of the fastest untethered insect-scale terrestrial robots. The CoT of the S²worm is also at an acceptable living insect level. The comparison Table V including several selected untethered robot [4], [10], [11], [35] proves that the S²worm is one of the best for speed and autonomous.

IV. Conclusion and Future Works

In this paper, we present S²worm, an untethered insect-scale inchworm robot with a novel 2-DoF transmission and integrated electronics to achieve high mobility. The 2-DoF transmission is designed by screw theory and fabricated by the SCM method. An onboard controller and a high voltage boost converter are achieved for communicating and driving the double deck PZT actuator. The S²worm weighs 4.34 g and spans 4.1 cm in length. Attributing to the design and fabrication method, the velocity of the robot is up to 27.4 cm/s, equivalent to 6.7 body length per second. The mobility is also exemplified by the turning test. The minimum turning radius of the S²worm reaches 1.7 cm, equivalent to 0.4 body length. The experimental results indicate that the S²worm holds high level autonomy, high mobility and high energy efficiency.

To the best of our knowledge, it is the first time to introduce the screw theory to design the parallel transmission mechanism of an insect-scale robot. According to the design and fabrication process of our work, the planarization of the SCM process shows high dependently with the limb design from the screw theory. It is proved that the linear combination of the limb can highly influence the following kinematic pair of the fabrication structure.

Our previous work on the BioARS system, has already proven that the inchworm like robot can be assembled into a quadruped robot to walk. The S²worm is designed for constructing a BioARS system at insect scale.

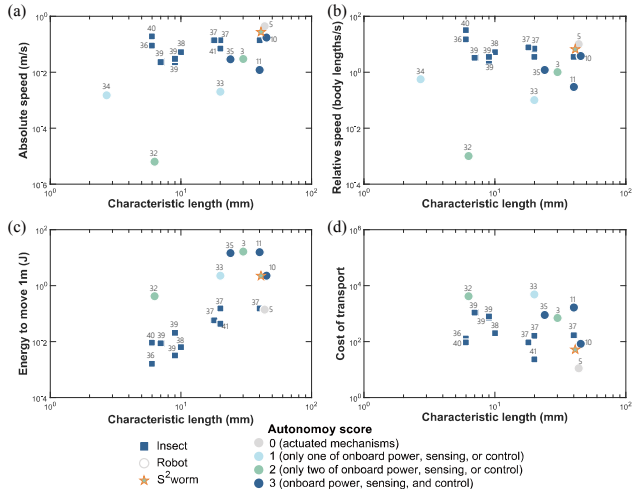

Fig. 7. Mobility and energy consumption parameters of selected robots and insects as a function of characteristic length. The numbers on the symbols earmark the sources of references. (a) Absolute speed. (b) Relative speed. (c) Energy to move 1m. (d) Cost of Transport.

TABLE IV
ENERGY REQUIRED TO MOVE 1M AND COST OF TRANSPORT

No.	Speed (cm/s)	Frequency (Hz)	Current (mA)
1	10.6	50	115
2	17.9	50	146
3	27.4	60	165
No.	**Power (mW)**	**Energy to move 1m (J)**	**Cost of transport**
1	425.5	4.01	94.4
2	540.2	3.00	70.5
3	610.5	2.23	52.4

TABLE V
COMPARISON BETWEEN THIS WORK AND THE OTHER SELECTED UNTETHERED ROBOTS

Name	Size (cm)	Weight (g)	Speed (cm/s)	Relative Speed (bl/s)	Cost of Transport
DASH [4]	10	16.2	150	15	14.7
HAMR-F [10]	4.5	2.8	17.2	3.8	83.9
DEAnsect [11]	4	0.97	1.2	0.3	1670 (Total)
Liang et al [35]	2.4	1.9	2.88	1.2	887 (Without sensor)
This work	4.1	4.34	27.4	6.7	52.4

Acknowledgment

The authors thank Chenyang Wang, Hejinsheng Cao, Ying Chen, Jichong Liu and Ji Tang for their help and suggestions.

References

[1] J.-S. Koh and K.-J. Cho, "Omegabot : Biomimetic inchworm robot using SMA coil actuator and smart composite microstructures (SCM)," in *2009 IEEE International Conference on Robotics and Biomimetics (ROBIO)*, 2009, pp. 1154–1159.

[2] R. J. Wood, "The First Takeoff of a Biologically Inspired At-Scale Robotic Insect," *IEEE Transactions on Robotics*, vol. 24, no. 2, pp. 341–347, Apr. 2008.

[3] A. M. Hoover, E. Steltz, and R. S. Fearing, "RoACH: An autonomous 2.4g crawling hexapod robot," in *2008 IEEE/RSJ International Conference on Intelligent Robots and Systems*, 2008, pp. 26–33.

[4] P. Birkmeyer, K. Peterson, and R. S. Fearing, "DASH: A dynamic 16g hexapedal robot," in *2009 IEEE/RSJ International Conference on Intelligent Robots and Systems*, 2009, pp. 2683–2689.

[5] A. T. Baisch, O. Ozcan, B. Goldberg, D. Ithier, and R. J. Wood, "High speed locomotion for a quadrupedal microrobot," *The International Journal of Robotics Research*, vol. 33, no. 8, pp. 1063–1082, Jul. 2014.

[6] R. St. Pierre and S. Bergbreiter, "Toward Autonomy in Sub-Gram Terrestrial Robots," *Annual Review of Control, Robotics, and Autonomous Systems*, vol. 2, no. 1, pp. 231–252, 2019.

[7] P. Bhushan and C. Tomlin, "An Insect-Scale Self-Sufficient Rolling Microrobot," *IEEE Robotics and Automation Letters*, vol. 5, no. 1, pp. 167–172, 2020.

[8] P. Bhushan and C. J. Tomlin, "Design of the First Sub-Milligram Flapping Wing Aerial Vehicle," in *2019 IEEE 32nd International Conference on Micro Electro Mechanical Systems (MEMS)*, 2019, pp. 2–5.

[9] C. Wang, W. Zhang, Y. Zou, R. Meng, J. Zhao, and M. Wei, "A Sub-100 mg Electromagnetically Driven Insect-inspired Flapping-wing Micro Robot Capable of Liftoff and Control Torques Modulation," *J Bionic Eng*, vol. 17, no. 6, pp. 1085–1095, Nov. 2020.

[10] B. Goldberg, R. Zufferey, N. Doshi, E. F. Helbling, G. Whittredge, M. Kovac, and R. J. Wood, "Power and Control Autonomy for High-Speed Locomotion With an Insect-Scale Legged Robot," *IEEE Robotics and Automation Letters*, vol. 3, no. 2, pp. 987–993, Apr. 2018.

[11] X. Ji, X. Liu, V. Cacucciolo, M. Imboden, Y. Civet, A. E. Haitami, S. Cantin, Y. Perriard, and H. Shea, "An autonomous untethered fast soft robotic insect driven by low-voltage dielectric elastomer actuators," *Science Robotics*, vol. 4, no. 37, Dec. 2019.

[12] T. Li, Z. Zou, G. Mao, X. Yang, Y. Liang, C. Li, S. Qu, Z. Suo, and W. Yang, "Agile and Resilient Insect-Scale Robot," *Soft Robotics*, vol. 6, no. 1, pp. 133–141, Nov. 2018.

[13] X. Yang, L. Chang, and N. O. Pérez-Arancibia, "An 88-milligram insect-scale autonomous crawling robot driven by a catalytic artificial muscle," *Science Robotics*, vol. 5, no. 45, Aug. 2020.

[14] D. S. Contreras, D. S. Drew, and K. S. J. Pister, "First steps of a millimeter-scale walking silicon robot," in *2017 19th International Conference on Solid-State Sensors, Actuators and Microsystems (TRANSDUCERS)*, 2017, pp. 910–913.

[15] A. T. Baisch, C. Heimlich, M. Karpelson, and R. J. Wood, "HAMR3: An autonomous 1.7g ambulatory robot," in *2011 IEEE/RSJ International Conference on Intelligent Robots and Systems*, 2011, pp. 5073–5079.

[16] J. P. Whitney, P. S. Sreetharan, K. Y. Ma, and R. J. Wood, "Pop-up book MEMS," *J. Micromech. Microeng.*, vol. 21, no. 11, p. 115021, Oct. 2011.

[17] K. Jayaram, J. Shum, S. Castellanos, E. F. Helbling, and R. J. Wood, "Scaling down an insect-size microrobot, HAMR-VI into HAMR-Jr," in *2020 IEEE International Conference on Robotics and Automation (ICRA)*, 2020, pp. 10305–10311.

[18] A. M. Mehta and K. S. J. Pister, "Flexure-Based Two Degree-of-Freedom Legs for Walking Microrobots," presented at the ASME 2006 International Mechanical Engineering Congress and Exposition, 2007, pp. 441–450.

[19] D. S. Contreras and K. S. J. Pister, "Durability of silicon pin-joints for microrobotics," in *2016 International Conference on Manipulation, Automation and Robotics at Small Scales (MARSS)*, 2016, pp. 1–6.

[20] D. S. Contreras and K. S. J. Pister, "Dynamics of electrostatic inchworm motors for silicon microrobots," in *2017 International Conference on Manipulation, Automation and Robotics at Small Scales (MARSS)*, 2017, pp. 1–6.

[21] J. Greenspun and K. S. J. Pister, "FIRST LEAPS OF AN ELECTROSTATIC INCHWORM MOTOR-DRIVEN JUMPING MICROROBOT," in *2018 Solid-State, Actuators, and Microsystems Workshop Technical Digest*, Hilton Head, South Carolina, USA, 2018, pp. 159–162.

[22] R. St. Pierre, W. Gosrich, and S. Bergbreiter, "A 3D-printed 1 mg microrobot running at 15 body lengths per second," in *2018 Solid-State, Actuators, and Microsystems Workshop Technical Digest*, Hilton Head, South Carolina, USA, 2018, pp. 59–62.

[23] Y. Liu, D. Zhao, Y. Chen, D. Wang, Z. Wen, Z. Ye, J. Guo, H. Zhou, S. Qu, and W. Yang, "BioARS: Designing Adaptive and Reconfigurable Bionic Assembly Robotic System with Inchworm Modules," in *2020 IEEE/RSJ International Conference on Intelligent Robots and Systems (IROS)*, 2020, pp. 11681–11687.

[24] J.-P. Merlet, "Parallel Robots: Open Problems," in *Robotics Research*, London, 2000, pp. 27–32.

[25] D. Zlatanov, "A Family of New Parallel Architectures with Four Degrees of Freedom," *Electronic Journal of Computational Kinematics*, vol. 1, pp. 1–10, 2001.

[26] K. H. Hunt, K. H. Hunt, and K. H. Hunt, *Kinematic geometry of mechanisms*, vol. 7. Oxford University Press, USA, 1978.

[27] R. S. Ball, *A Treatise on the Theory of Screws*. Cambridge university press, 1998.

[28] Z. Huang and Q. C. Li, "Type Synthesis of Symmetrical Lower-Mobility Parallel Mechanisms Using the Constraint-Synthesis Method," *The International Journal of Robotics Research*, vol. 22, no. 1, pp. 59–79, Jan. 2003.

[29] Z. Huang and Q. C. Li, "General Methodology for Type Synthesis of Symmetrical Lower-Mobility Parallel Manipulators and Several Novel Manipulators," *The International Journal of Robotics Research*, vol. 21, no. 2, pp. 131–145, Feb. 2002.

[30] H. Suzuki and R. J. Wood, "Origami-inspired miniature manipulator for teleoperated microsurgery," *Nat Mach Intell*, vol. 2, no. 8, pp. 437–446, Aug. 2020.

[31] R. J. Wood, E. Steltz, and R. S. Fearing, "Optimal energy density piezoelectric bending actuators," *Sensors and Actuators A: Physical*, vol. 119, no. 2, pp. 476–488, Apr. 2005.

[32] S. Hollar, A. Flynn, C. Bellew, and K. S. J. Pister, "Solar powered 10 mg silicon robot," in *IEEE The Sixteenth Annual International Conference on Micro Electro Mechanical Systems, 2003. MEMS-03 Kyoto*, 2003, pp. 706–711.

[33] M. Qi, Y. Zhu, Z. Liu, X. Zhang, X. Yan, and L. Lin, "A fast-moving electrostatic crawling insect," in *2017 IEEE 30th International Conference on Micro Electro Mechanical Systems (MEMS)*, 2017, pp. 761–764.

[34] K. Saito, K. Sugita, Y. Ishihara, K. Iwata, Y. Asano, Y. Okane, S. Ono, S. Chiba, M. Takato, and F. Uchikoba, "Insect-type MEMS microrobot with mountable bare chip IC of artificial neural networks," *Artif. Life Robot.*, vol. 22, no. 1, pp. 118–124, Mar. 2017.

[35] J. Liang, Y. Wu, J. K. Yim, H. Chen, Z. Miao, H. Liu, Y. Liu, Y. Liu, D. Wang, W. Qiu, Z. Shao, M. Zhang, X. Wang, J. Zhong, and L. Lin, "Electrostatic footpads enable agile insect-scale soft robots with trajectory control," *Science Robotics*, vol. 6, no. 55, Jun. 2021.

[36] A. Lipp, H. Wolf, and F.-O. Lehmann, "Walking on inclines: Energetics of locomotion in the ant Camponotus," *The Journal of experimental biology*, vol. 208, pp. 707–19, Mar. 2005.

[37] R. Full, D. Zuccarello, and A. Tullis, "Effect of variation in form on the cost of terrestrial locomotion," *The Journal of experimental biology*, vol. 150, pp. 233–46, Jun. 1990.

[38] J. R. B. Lighton, G. A. Bartholomew, and D. H. Feener, "Energetics of Locomotion and Load Carriage and a Model of the Energy Cost of Foraging in the Leaf-Cutting Ant Atta colombica Guer," *Physiological Zoology*, vol. 60, no. 5, pp. 524–537, Sep. 1987.

[39] T. F. Jensen and I. Holm-Jensen, "Energetic cost of running in workers of three ant species,Formica fusca L.,Formica rufa L., andCamponotus herculeanus L. (Hymenoptera, Formicidae)," *J Comp Physiol B*, vol. 137, no. 2, pp. 151–156, Jun. 1980.

[40] L. Reinhardt and R. Blickhan, "Level locomotion in wood ants: evidence for grounded running," *Journal of Experimental Biology*, vol. 217, no. 13, pp. 2358–2370, Jul. 2014.

[41] J. H. Fewell, J. F. Harrison, J. R. B. Lighton, and M. D. Breed, "Foraging energetics of the ant, Paraponera clavata," *Oecologia*, vol. 105, no. 4, pp. 419–427, Mar. 1996.